Water Science & Technology

IWA PUBLISHING

Water Science & Technology Vol 84 No 9, 2394 doi: 10.2166/wst.2021.435

Isotherm and selectivity study of Ni(II) removal using natural and acid-activated nanobentonites

Zahra Ashouri Mehranjani[a], Majid Hayati-Ashtiani[a,*] and Mehran Rezaei[b]

[a] Department of Chemical Engineering, Faculty of Engineering, University of Kashan, Kashan, Iran
[b] School of Chemical, Petroleum and Gas Engineering, Iran University of Science and Technology (IUST), Tehran, Iran
*Corresponding author. E-mail: hayati@kashanu.ac.ir

ABSTRACT

In this research, natural bentonite and its acid-activated forms were employed as adsorbents for the adsorption of Ni^{2+} ions from wastewater. Natural bentonite was activated with 2 M sulfuric acid, 4.5 h and 95 °C (the best acid-activated sample with the highest adsorption capacity) and the other 6 M sulfuric acid, 7.5 h and 95 °C (the worst acid-activated sample with the lowest adsorption capacity). The adsorption of Ni^{2+} was studied through experiments including equilibrium contact time and selectivity. The equilibrium contact time for bentonite was obtained at 180 min. The Ni^{2+} separation process along with Zn^{2+} selectivity studies was considered through adsorption experiments. The results showed that there was a maximum amount of Ni^{2+} adsorption in the absence of Zn^{2+} for all samples. The results showed the best fit is obtained with the pseudo-second-order kinetic model. Working out different bentonite types to determine the best kinetic models, we explored the Langmuir and Florry–Huggins models provided a good fit with experimental data for acid-activated bentonites and the best results from linear forms of the adsorption isotherm models for fitting the experimental data of natural bentonite are obtained for Langmuir, Temkin and Freundlich models.

Key words: acid-activated, bentonite, nanoporous, nickel, selectivity

HIGHLIGHTS

- Working out different nanobentonite types to determine the best kinetic models.
- Investigating special acid-activated nanobentonite through Ni adsorption isotherms.
- New approach to study Ni separation process through a modeling provided.

NOMENCLATURE

Symbol	Meaning	Units
q_t	amount of Ni^{2+} adsorbed per unit mass of adsorbent at any time t	mg/g
q_e	adsorption capacity at equilibrium	mg/g
C_e	equilibrium concentration of Ni^{2+} in solution	mg/L
C_0	initial concentration of the Ni^{2+} solution	mg/L
C_t	liquid-phase concentrations of the Ni^{2+} solution at any time t	mg/L
m_s	amount of adsorbent used	g
K_1	rate constant of pseudo-first-order	min^{-1}
K_2	rate constant of pseudo-second-order	min^{-1}
K_{fd}	the film diffusion adsorption capacity	min^{-1}
K_{id}	intraparticle diffusion rate constant	min^{-1}
α	related to rate of chemisorption (initial adsorption rate)	–
β	desorption constant that is related to surface coverage	–

(*Continued*)

Symbol	Meaning	Units
K_f	Freundlich isotherm constant related to adsorption capacity	$(mg/g)(L/mg)^{1/n}$
n_f	Freundlich isotherm constant related to adsorption intensity	–
Q_m	maximum adsorption at monolayer coverage	mg/g
b	constant related to the extent of adsorption	L/mg
b_T	Temkin heat of adsorption	kJ/mol
B_T	Temkin isotherm energy constant	–
A_T	Temkin adsorption potential	L/mg
Q_{DR}	D–R adsorption capacity	mg/g
γ	D–R adsorption energy constant	mol^2/kJ^2
ε	Polanyi potential	–
E	adsorption energy	kJ/mol
R	gas constant	J/mol.K
T	absolute temperature	K
K_{FH}	equilibrium constant	min^{-1}
θ	the degree of surface coverage	–

1. INTRODUCTION

Bentonites are from aluminosilicate three-layer clays, belonging to the smectite group, which consists of several clay minerals like montmorillonite. The montmorillonite is a nanostructured 2:1 layer mineral consisting of the aluminum octahedral sheet sandwiched between two silica tetrahedral sheets (Ghazizahedi & Hayati-Ashtiani 2018). The substitution of exchangeable cations with molecules of water results in the increase of interlayer spacing depending on exchangeable cation types (Hayati-Ashtiani *et al.* 2011). Bentonites are known for their properties such as relatively high specific surface area, high cation exchange capacity, swelling, adsorption capacity, chemical and mechanical stability (Darvishi & Morsali 2011; Ostovaritalab & Hayati-Ashtiani 2019). The results of acid activation are amorphous silica production, nanoporous bentonite, influencing in surface area, average pore volume, cation exchange capacity and surface acidity (Temuujin *et al.* 2004). These changes depend on several factors including acid concentration, activation time and temperature, particle size distribution, etc. (Salem & Karimi 2009; Leroy *et al.* 2017). In our studies, the effects of sulfuric acid concentration and activation time on the acid-activation process of bentonite have been studied and the other parameters are considered constants.

Nickel is entered into the environment as one of the heavy metals through industrial processes such as nickel alloys, processing of mineral, electroplating, etc. The toxicity of nickel causes of diseases such as chronic bronchitis (by metallic nickel), emphysema (by nickel(II)), impaired lung function and lung cancer (by nickel(II)). Therefore, it is necessary to remove nickel from wastewaters. Bentonites and their modification are more studied rather than other adsorbents for nickel removal due to their specific characteristics, easy availability and less cost (Bhattacharyya & Gupta 2008; Li *et al.* 2017).

The adsorption of toxic metal Ni on natural, pillared and acid-activated montmorillonite has been described by researchers. The kinetics study of the removal of Ni(II) from aqueous solution on the Na-montmorillonite showed that equilibrium for Ni(II) onto Na-montmorillonite was reached in 200 min, and the adsorption of Ni(II) was pH dependent in the pH range 2–9 (Hayati-Ashtiani & Azimi 2016). The effects of modified adsorbents have been studied and the adsorption of nickel increased by acid activation (Bhattacharyya & Gupta 2008) and thermal treatment of bentonites (García-Carvajal *et al.* 2019). The equilibrium results of nickel adsorption on bentonite can be described using different adsorption isotherm models (Bhattacharyya & Gupta 2008; Ghomri *et al.* 2013), pseudo-first and pseudo-second orders (Yağmur 2020), and Elovich and pseudo-second-order equations (Iqbal *et al.* 2019; Tang *et al.* 2021). Other researchers' studies also showed that pseudo-second-order kinetic models revealed better agreement with kinetic experimental data as matched with other kinetic models (Imran *et al.* 2021). While the adsorption kinetics and isotherms of acid-activated bentonites have not received much attention, this research has studied them.

This study primary aim was investigating the application of nanoporous and nanostructured bentonite in removing nickel from aqueous solutions through experimental and instrumental analyses along with isotherm modeling and selectivity studies to define the adsorption properties of natural and acid-activated bentonites. The experimental and instrumental analyses include acid activation, adsorption experiments, selectivity study, scanning electron microscopy (SEM), X-ray diffraction (XRD), Fourier transform infrared (FTIR) spectroscopy, and pore size measurement. The first novel insight provided was the above-mentioned characterization experiments which yielded some significant results which showed the adsorption characteristics of the natural bentonite and the best and worst types of acid-activated bentonite to be used for the adsorption of Ni(II). Further, since natural and acid-activated bentonites have different characterizations, the kinetic and isotherm models have been applied with different new insights.

2. MATERIALS AND METHODS

2.1. Materials

Natural bentonites were provided from Ghaen Zarinkhak company (Khorasan Razavi Province, Iran) and other chemicals including nickel nitrate ($Ni(NO_3)_2.6H_2O$, 99%), zinc nitrate ($Zn(NO_3)_2.6H_2O$, 98%), and sulfuric acid (H_2SO_4, d = 1.84, 96%) and nitric acid (HNO_3, d = 1.4, 65%) were purchased from Merck Chemicals. The standard solutions of stocks were prepared with distilled water. Bentonites have been modified by acid treatment in a shaking water bath with 50 g of bentonite dispersed in 1,000 mL of 2 M H_2SO_4 for 4.5 h at 95 °C (B1 sample) and 6 M H_2SO_4 for 7.5 h at 95 °C (B2 sample). The suspension was washed with distilled water, and also dried at 105 ± 5 °C for 16 h.

2.2. Acid-activation method

To prepare acid-activated bentonite by sulfuric acid, bentonite passed through sieve mesh No. 200 was first dried at 110 °C. For acid activation, 50 g of bentonite was weighed and homogenized with 1,000 ml of sulfuric acid solution. The effect of acid concentration and bentonite contact time factors on the quality of activated bentonite was investigated. To evaluate the effect of sulfuric acid concentration, concentrations of 1, 2, 3, 4, 5 and 6 M were used during contact times of 1.5, 3, 4.5, 6 and 7.5 h. The product obtained after crushing was used to determine the adsorption of Ni^{2+}. Finally, the best and worst activated samples with the highest and lowest nickel uptake were named B1 and B2, respectively.

2.3. Characterizations

A LEO 1450 VP SEM equipped with energy-dispersive X-ray (EDAX) spectroscopy was used for morphological characterizations of the sample. SEM system works at 30 kV of electron accelerating maximum voltage and has a LaB6 filament and maximum spot magnification of ×20,000. Mineralogy analyses were performed with a STOE STADIMP diffractometer equipped with a graphite secondary monochromator to evaluate the sample by XRD. A Vector 22 Bruker FT–IR spectrometer recorded spectra on the spectral range of 4,000–400 cm^{-1}. Bentonite samples were prepared at with a fixed amount of clay and KBr to obtain 13 mm diameter pellets. The pellets were heated overnight at 110 °C to remove adsorbed water before recording the spectra. The pore size distribution of bentonites was determined from desorption isotherms using the Quantachrome NOVA 2000e series volumetric gas adsorption instrument and the Barrett–Joyner–Halenda (BJH) method.

2.4. Adsorption experiments

The stock solution of Ni^{2+} was prepared for adsorption experiments by dissolving an appropriate quantity of $Ni(NO_3)_2.6H_2O$. The stock solution was diluted with distilled water to 200 ppm. After preparation of the solution, effective parameters on the adsorption of Ni were studied on natural bentonite, B1 which was the best activated sample (2 M of H_2SO_4 for 4.5 h at 95 °C) had the highest amount of nickel adsorption and B2 which was the worst activated sample (6 M of H_2SO_4 for 7.5 h at 95 °C) had the lowest amount of nickel adsorption. After each reaction, solution samples were separated from the bentonite by filtration followed and the filtrate residual of Ni^{2+} cations was analyzed using ICP.

2.4.1. Selectivity study

The purpose of the selectivity experiment was the separation of nickel from a solution of nickel–zinc. The choice of zinc for adsorption experiments has been made because of the presence of zinc with nickel in industrial wastewaters. Therefore, zinc was considered as the intruder ion for adsorption process. For this purpose, the stock solutions were prepared to 200 ppm from both metals. Experiments were performed by taking 0.3 g from each of the samples and making a 25 mL solution. The experiments were carried out at concentrations of 180, 160, 140, 120 for nickel and 20, 40, 60, 80 and 100 ppm for

zinc solution in which the specific values of 200 ppm solution of both ions were added. For example, 22.5 ml of nickel solution and 2.5 ml of zinc solution at 200 ppm were added for a 20 ppm concentration of zinc and 180 ppm concentration of nickel.

The adsorption amount of nickel was studied as a function of time for adsorption kinetics with 25 ml of 200 ppm nickel solution that was mixed with 0.3 g bentonite at 25 °C and completely shaken at 150 rpm for various times from 30 s to 4 h.

To explain the kinetic experiments, the results of Ni adsorption on bentonite can be presented through different kinetic models including pseudo-first-order, pseudo-second-order, intraparticle diffusion (Weber–Morris), and Elovich equation. The kinetic models are briefly mentioned in Equations (1)–(5) (Ijagbemi *et al.* 2010; Malamis & Katsou 2013):

$$\text{Pseudo-first-order: } \ln(q_e - q_t) = \ln(q_e) - K_1 t \tag{1}$$

$$\text{Pseudo-second-order: } \frac{t}{q_e} = \frac{1}{(K_2 q_e^2)} + \frac{t}{q_e} \tag{2}$$

$$\text{Elovich equations: } q_t = \frac{1}{\beta \ln(\alpha\beta)} + \frac{1}{\beta \ln(t)} \tag{3}$$

$$\text{Intraparticle diffusion (Weber–Morris): } q_t = K_{id} t^{0.5} \tag{4}$$

$$\text{Liquid film diffusion: } \ln\left(1 - \frac{q_t}{q_e}\right) = -K_{fd} t \tag{5}$$

where:

$$q_t = \frac{(C_0\text{-}C_t)(V/1{,}000)}{m_s} \tag{6}$$

2.5. Adsorption isotherm models

The batch adsorption experiments were conducted taking 0.3 g of the adsorbent with 25 mL of nickel solution at different concentrations, namely, 50, 100, 150, 200, 250, 300 and 350 ppm at 25 °C and completely shaken at 150 rpm for 4 h. The equilibrium data of Ni^{2+} adsorption on natural and acid-activated bentonites were presented using different adsorption isotherm models including Freundlich, Langmuir, Temkin, Dubinin–Radushkevich (D–R), and Florry–Huggins equations, which are in Table 1.

The Freundlich adsorption isotherm was used to describe the heterogeneous surface, reversible adsorption and surface with different bonding. This model assumes that the site is occupied by a stronger bond and the bond strength decreases, increasing the degree of occupation of the site. $1/n_F$ is the heterogeneity factor which varies between 0 and 1. If the value of n_F is below unity, which means n_F is between 1 and 10, it suggests that we have a chemical adsorption process, and if n_F is above unity, we have physical adsorption. The Langmuir model is based on the assumption of monolayer adsorption onto a homogeneous surface. The factor of this model implied the interaction between the adsorbent and the adsorbed species by assumption of a linear decrease in energy adsorption. The D–R model was used to describe the physical and chemical characteristics of the adsorption

Table 1 | Isotherm models

	Equation	Linear form of equation
Freundlich	$q_e = k_f C_e^{1/n_f}$	$\ln q_e = \ln k_f + 1/n_f \ln C_e$
Langmuir	$q_e = \frac{Q_m k_1 C_e}{1 + k_1 C_e}$	$\frac{C_e}{q_e} = \frac{1}{bQ_m} + \frac{C_e}{Q_m}$
Temkin	$q_e = \frac{RT}{b_T} \ln(A_T C_e)$	$q_e = B_T \ln(A_T) + B_T \ln(C_e)$
Dubinin–Radushkevich	$\ln(q_e) = \ln(Q_{DR}) - \gamma\varepsilon^2$	The same
Florry–Huggins	$\log\left(\frac{\theta}{C_0}\right) = \log(k_{FH}) + \lambda \log(1-\theta)\theta = \left(1 - \frac{C_e}{C_0}\right)$	The same

of nickel on bentonite, estimating the characteristic porosity of the adsorbent and the adsorption energy. The Florry–Huggins model is characterized by the degree of coverage of the adsorbent to adsorb on the surface (Dada *et al.* 2012).

3. RESULTS

3.1. Characterizations

The SEM of samples are shown in Figure 1(a) (magnification ×5,000), 1(b) (magnification ×10,000), 1(c) (magnification ×15,000), and 1(d) (magnification ×20,000). Bentonites have heterogeneous particles with sizes ranging from several μm to nm. The particle surfaces clearly display a wavy, fuzzy and crumpled appearance, showing the presence of montmorillonite. Montmorillonite is highly honeycombed in nature and exhibits a large agglomerates of very fine particles. Figure 1(a)–1(d) shows the surface morphology of samples and indicates a layered structure of montmorillonite. For the individual particles, most of them have clearly irregular platelets but tend to form some thick and large agglomerates, especially as seen in Figure 1(a). This SEM photograph highlight the shape of montmorillonite as a sponge-like appearance with irregular structure and open voids in the surface morphology, where the surface is unsmooth.

Figure 2 shows that the XRD patterns of B0, B1, and B2 are nearly identical, but there are a few notable increases or decreases in some 2θ peak intensities. The peak intensity decreased at about $2\theta = 8$–$10°$. The decrease is considerable for sample B2 which is activated in the presence of 6 M sulfuric acid. The intensity at about $2\theta = 20$–$25°$ increased. The intensities of peaks in samples B1 (4M and 4.5 h) and B2 (6 M and 7.5 h) are decreased slightly.

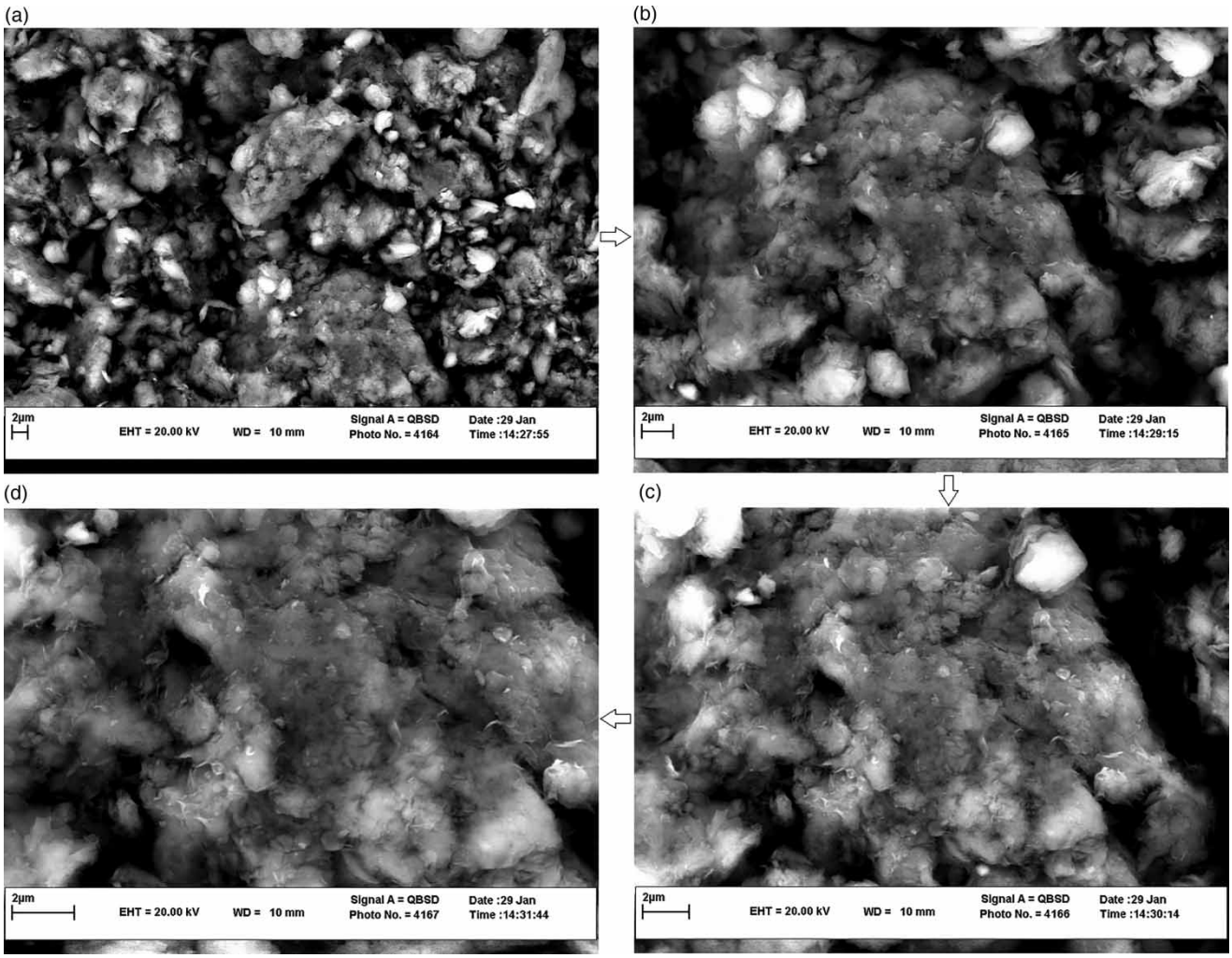

Figure 1 | SEMs of sample at increasing magnifications (a) ×5,000, (b) ×10,000, (c) ×15,000, (d) ×20,000.

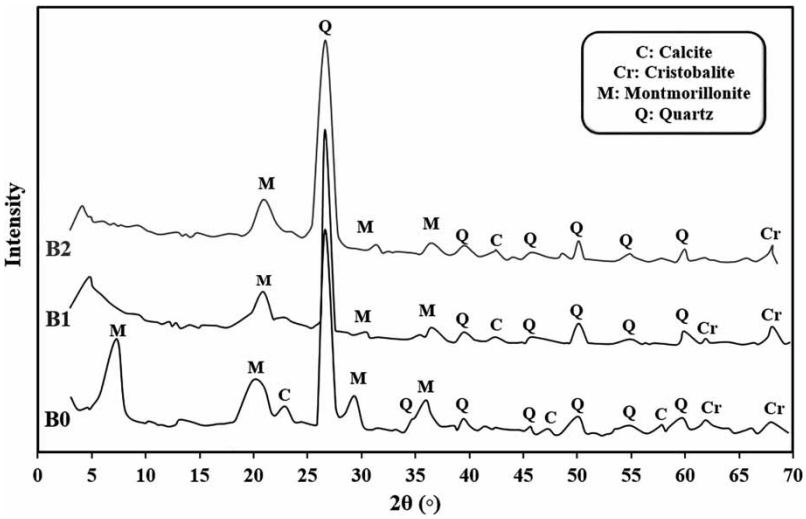

Figure 2 | The XRD patterns of natural and acid-activated bentonites.

Figure 3 shows FTIR analyses of samples. FTIR analysis is a useful method to figure out the structure, bonding and chemical properties of clay minerals. In all samples, there are adsorption bands in the ranges 3,640–3,400 cm^{-1}, 1,640–1,430 and most of the bands are at 1,100–460 cm^{-1}. There is the band near 1,090 cm^{-1} just in acid-activated samples B1 and B2.

The results showed that the intensities of the absorption bands at 3,625, 1,430, 1,048, 926, 875, 835, 625 and 510 cm^{-1} are decreased in B1 and B2 and absorption band almost disappeared in sample B2. The adsorption bands at 875 cm^{-1} can be observed in B0, but this adsorption band was not observed in B1 and B2. As can be seen, the adsorption band at 835 cm^{-1} was not observed in sample B2.

BJH analysis is usually a good method to determine the pore size and volume distribution of adsorbents (Hayati-Ashtiani 2011). Table 2 shows the pore diameter and volume of the samples. The results revealed that the activated samples exhibited higher pore volume and smaller pore size compared to natural bentonite. Among the activated samples, the B1 sample exhibited the highest pore diameter and volume.

3.2. Selectivity study

There is another important factor that affects the Ni^{2+} adsorption on natural and activated bentonite. The effect of the presence of Zn^{2+} on the nickel adsorption is shown in Figure 4. Zn and Ni are indicated after the name of sample in the legend of Figure 4 and the horizontal axis shows Zn or Ni metal concentrations in mg/l. The results show that there is a maximum

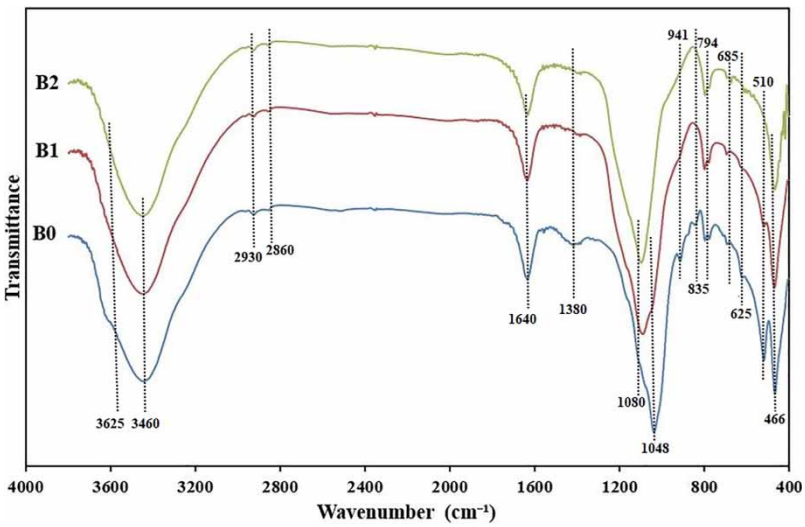

Figure 3 | FTIR spectra curves of natural and acid-activated bentonites.

Table 2 | The textural properties of natural and acid-activated bentonites

Sample	Pore diameter (nm)	Pore volume (cm^3/g)
B0	2.72	0.03
B1	1.20	0.32
B2	1.19	0.23

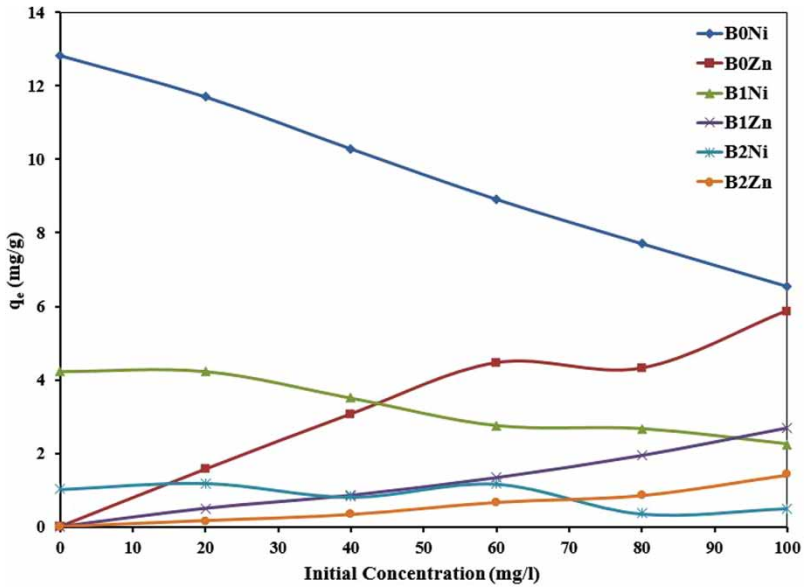

Figure 4 | Effect of the presence of Zn^{2+} ions in solution on the adsorption of Ni^{2+} for all samples.

amount of Ni^{2+} adsorption in the absence of Zn^{2+} for all samples, since Zn^{2+} cations compete with Ni^{2+} cations for adsorption in bentonite surfaces. Therefore, the maximum amount of Ni^{2+} adsorption (q_e) was observed in the absence of Zn^{2+} for all samples. Also, the uptake of Ni^{2+} decreased with increase in the Zn^{2+} concentration. As can be seen, the highest amounts of nickel and zinc adsorption were observed for B0 and B1, respectively. For all samples, Ni^{2+} adsorption curves are almost located above the Zn^{2+} adsorption curves. In sample B1, adsorption curves crossed the Zn^{2+} concentration of 90 ppm and then the result is reversed. The same cross took place at the Zn^{2+} concentration of 70 ppm for sample B2.

3.3. Adsorption kinetics

Figure 5 shows the effect of contact time on the adsorption of nickel. The adsorption increased with time up to 150 min and then almost remained constant. The adsorption amount was rapid up to 50 min and then there was a small decrease until the adsorption process reached an equilibrium. The experimental data were fitted with different models for testing the kinetics of Ni^{2+} adsorption on bentonite.

The pseudo-first-order kinetic model curve was attained by plotting $\ln(q_e - q_t)$ versus time. The curve of the pseudo-first-order kinetic model was linear ($R^2 = 0.34$) and the first-order rate coefficient was obtained from the slope ($K_1 = 0.01$). The amount of the Ni equilibrium adsorbed obtained ($q_e = 2.01$ mg/g) by the pseudo-first-order kinetic model was different compared to the experimental q_e value ($q_e = 12.5$ mg/g). First-order kinetics is not suitable for describing the Ni adsorption kinetic. Among the applied models, the pseudo-second-order kinetic model with $R^2 = 0.99$, which was obtained by plotting t/q_t versus time was perfectly fitted with the Ni adsorption data. The q_e value was obtained ($q_e = 12$ mg/g) by the pseudo-second-order kinetic model and was almost equal to that of the experimental q_e value ($q_e = 12.5$).

The Elovich model, intraparticle diffusion and liquid film diffusion model, were used to fit the experimental data, which were not suitable for modeling Ni adsorption. The plot of the results of q_t vs. ln(t) for the Elovich kinetic model showed a

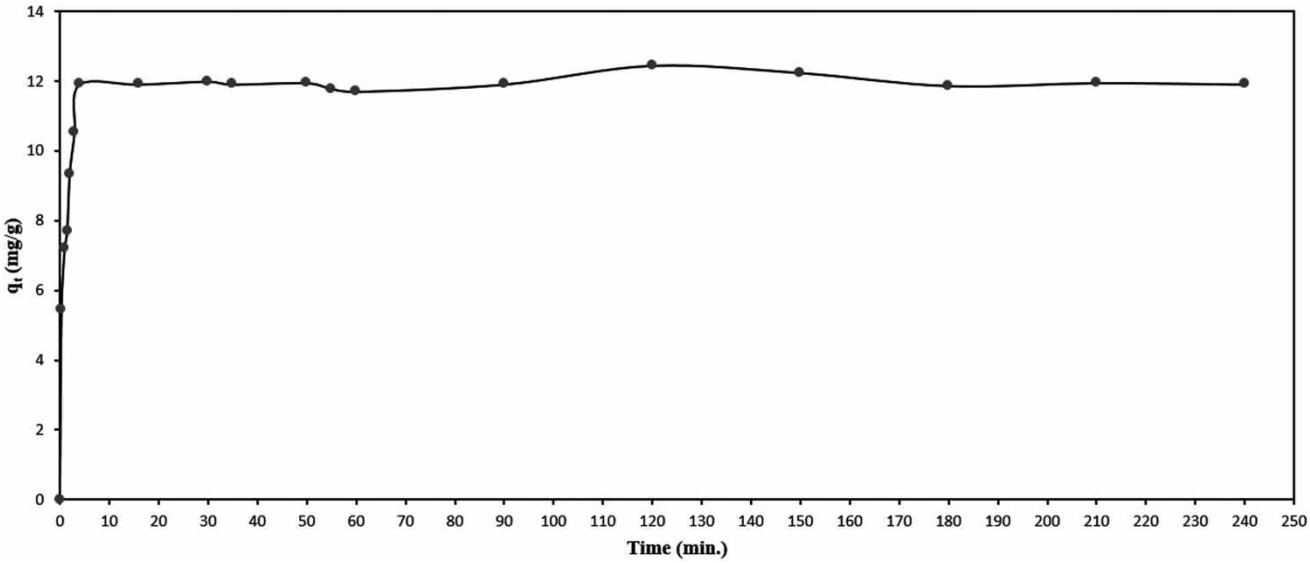

Figure 5 | Effect of contact time on Ni^{2+} adsorption by natural bentonite.

straight line ($R^2 = 0.63$). The value of the coefficients, α and β, were 316.56 and 0.83, respectively. Fitting the intraparticle diffusion equation to the Ni adsorption data (the plot of q_t vs. $t^{1/2}$) led to a relatively poor fit ($R^2 = 0.45$). The slope of the linear plot, defined as the intraparticle diffusion rate constant (k_{id}) was 0.43. The liquid film diffusion kinetic model curve obtained by plotting $\ln(1 - q_t/q_e)$ vs. time was linear ($R^2 = 0.34$) and the film diffusion rate coefficient, k_{fd}, had the value in 0.01 which was obtained from the slope of the plot. The calculated parameters were reported in Table 3.

3.4. Adsorption isotherm

The influence of the initial concentration on the adsorption of nickel is shown in Figure 6. It shows that, in the initiation step, the adsorption increases with increase in the initial concentration of Ni^{2+} for all samples. Figure 6 represents the highest amount of adsorption of Ni^{2+} for natural sample B0. There was an increase in the amount of adsorption of Ni^{2+} from 4.08 to 14.12 mg/g for sample B0. There was a sharp increase in the amount of adsorption of Ni^{2+} in the initiation step of adsorption up to the concentration 200 mg/l for natural sample B0. The same increase was observed for samples B1 and B2 but this increase was not as sharp as that of reported for natural sample B0.

Table 3 | The parameters calculated from kinetic models

Equation	Parameters	
Pseudo-first-order	K_1	0.01
	q_e	2.01
	R^2	0.34
Pseudo-second-order	K_2	0.33
	q_e	12
	R^2	0.99
Elovich equations	A	316.56
	β	0.83
	R^2	0.63
Intraparticle diffusion (Weber–Morris)	k_{id}	0.43
	R^2	0.45
Liquid film diffusion	K_{fd}	0.01
	R^2	0.34
Experimental	q_e	12.5

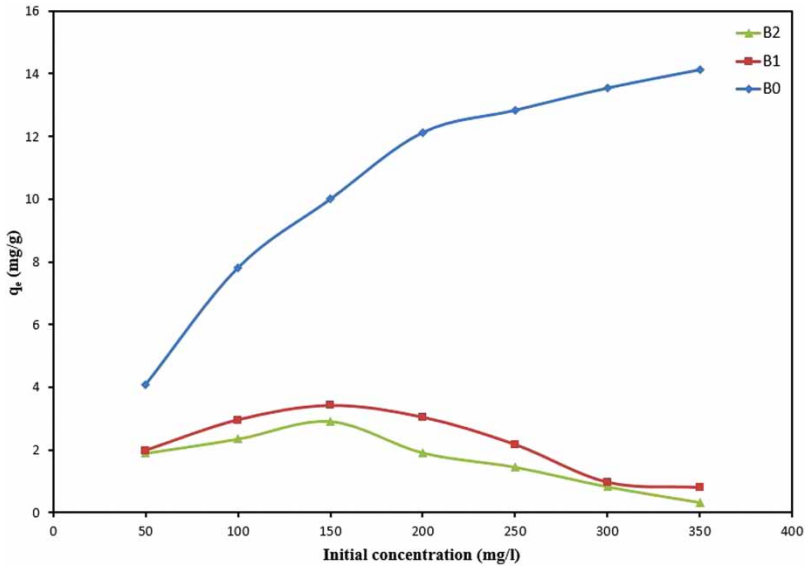

Figure 6 | Effect of initial concentration on Ni^{2+} adsorption.

The experimental data were fitted well into different models for testing the adsorption isotherm models of Ni^{2+} adsorption on bentonite and the resulting model parameters calculated from model equations are reported in Table 4.

For sample B0, the best fit for the experimental data may have to be adjusted to the Langmuir, Temkin and Freundlich models. The Langmuir model curve obtained by plotting c_e/q_e vs. c_e is linear ($R^2 = 0.996$) and the value of the parameters, Q_m and b, were 14.409 and 0.125, respectively. The Temkin model plot shows a linear curve with $R^2 = 0.993$ by plotting q_e vs. ln c_e and the Freundlich model curve was obtained from plotting ln q_e vs. ln c_e. The curve of the Freundlich model was linear ($R^2 = 0.971$) and the n_f value yielded above unity ($n_f = 4.344$) from the slope.

The experimental data for B1 and B2 are best described by the Florry–Huggins model, which is plotted as $\log(\theta/c_0)$ vs. $\log(1-\theta)$ and the data are fitted in a linear curve with $R^2 = 0.903$ and 0.861 for samples B1 and B2, respectively. The Florry–Huggins constant obtained $K_{FH} = 0.0001$ for the two samples.

The Dubinin–Radushkevich isotherm was not fitted to the adsorption of Ni^{2+} by all adsorbents, as the R^2 values were 0.814, 0.157 and 0.199 for samples B0, B1 and B2, respectively. The E values for the D–R model were obtained as 1.205, 0.464 and 0.336 kJ/mol for B0, B1 and B2, respectively.

Table 4 | The parameters calculated from adsorption isotherm models

Isotherm models	Parameters	B0	B1	B2
Freundlich	K_f	4.525	10.711	0.587
	n_f	4.344	2.861	0.338
	R^2	0.971	0.321	0.412
Langmuir	Q_m	14.409	0.782	0.388
	B	0.125	−0.015	−0.012
	R^2	0.996	0.835	0.669
Temkin	A_T	8.684	1.309×10^{-4}	4.689×10^{-4}
	B_T	1.910	−0.543	−0.610
	R^2	0.993	0.249	0.385
Dubinin–Radushkevich	γ	−0.344	−2.319	−4.416
	Q_{DR}	11.637	1.647	1.108
	E	1.205	0.464	0.336
	R^2	0.814	0.157	0.199
Florry–Huggins	λ	−0.757	−6.533	−8.431
	K_{FH}	0.001	0.0001	0.0001
	R^2	0.949	0.903	0.861

4. DISCUSSION

The main adsorption mechanisms are ion exchange between Ni^{2+} and benonite at pH < 7 and precipitation at pH > 7 if one wants to describe briefly what is the adsorption mechanism. The competition between the Ni^{2+} and H_3O^+ cations on the bentonite surface adsorption is the possible reason for the low adsorption of Ni^{2+} in the acidic regions. Also, the functional groups in the bentonite surfaces vary with protonation/deprotonation processes. The expected positive groups like H_3O^+ increases at acidic pH and the dominant adsorption process is ion exchange. The increase in pH increases the negative charge of the bentonite surface and leads to the increase of Ni^{2+} adsorption since the negative functional groups increases. As the pH is further increased to reach the basic region, the solubility of the metal decreases in solution and causes precipitation. So, the adsorption mechanism at high pH is precipitation (Ijagbemi *et al.* 2010).

The results of the selectivity study showed that the maximum adsorption of nickel for each sample is obtained in the absence of cations. The results show that an increase in concentrations of Zn^{2+} solution causes a reduction in Ni^{2+} adsorption. The results show that the adsorption capacity depends on the type and concentration of other cations in solution. Also, the number of competitive particles in solution increases with increasing concentrations of other cations while the adsorption active sites of the natural and activated bentonites are constant.

As adsorption on the adsorption site depends on the metal ions hydrated ionic radius, the cations with smaller hydrated ionic radii have easier approaches to the bentonite surface and they can penetrate more easily inside its pores. This suggests that competition and ion hydrated ionic radius are close together for these cations. The Ni^{2+} and Zn^{2+} hydrated radii are 0.404 and 0.430 nm, respectively compared B0, B1 and B2 pore diameters which are 2.72, 1.20 and 1.19 nm, respectively as stated in Table 2.

The results of kinetics revealed that the behavior of Ni^{2+} adsorption is similar to an H-shape curve which has a vertical shape at the initial step of the adsorption process that represents the rapid adsorption on the active available sites. Also, it was found that the first-order kinetic model does not have a suitable relation to describe the sorption rate of Ni^{2+} onto bentonite. But, the results indicate that the pseudo-second-order model can be fitted for adsorption of Ni^{2+} onto bentonite. The order of suitability of kinetics models for adsorption of Ni^{2+} onto bentonite is: pseudo-second-order > Elovich > Webber–Morris > pseudo-first-order and liquid film diffusion. Since the pseudo-second-order model describes the chemisorption reaction well, the adsorption process is complex and involves more than one mechanism and the chemical reaction may take place such that the valence force with the exchange of ions causes the formation of covalent bonds.

At the first initiation of 50 min, the adsorption was rapid because the active sites on the bentonite surface are numerous and the highest adsorption was obtained in this period. In this stage, the governing mechanism of adsorption is the mass transfer mechanism, which is the boundary layer diffusion to the bentonite external surface. Then, adsorption was slow as the external surface was filled by nickel cations. In this stage, for further interactions or reactions including ion exchange and complexation of Ni^{2+} ions, the adsorption is the diffusion of Ni^{2+} ions to pore and active particles of bentonite so that the adsorption occurred with diffusion or ion exchange processes. The adsorption slowed down until equilibrium adsorption was achieved.

This section describes kinetics obtained by Elovich equation, intraparticle diffusion and liquid film diffusion, but the adsorption and the correlation coefficients for these models were low. So, the mechanism of adsorption can be expressed by the first stage.

The study of the equilibrium data using adsorption isotherm models indicates that the adsorption of Ni^{2+} on natural bentonite corresponded to the Langmuir model. So, this confirms that the Ni^{2+} cations form a monolayer on the bentonite surfaces. Several other studies showed that the Langmuir and the Freundlich models have the best fit of the experimental data (Ghomri *et al.* 2013; Malamis & Katsou 2013). Since the dimensionless equilibrium parameter R_L (separation factor) of the Langmuir equation was between 0 and 1 for adsorption of Ni^{2+} on B0, Ni^{2+} adsorption on B0 was successful. Conversely, a n_F value for the Freundlich model that was between 1 and 10 in B0 indicates that the Ni^{2+} was physically adsorbed on the bentonite surfaces. Also, the value of $1/n_F$ is 0.23, which shows the amount of bentonite surface heterogeneity. Ni^{2+} adsorption on activated bentonite can be explained with the Florry–Huggins model. The λ value of Ni^{2+} adsorption amount on B1 was greater than that of B2 for the Florry–Huggins model. This shows that more Ni^{2+} was adsorbed on the active sites of the B1. The result reveals that B1 has better Ni^{2+}adsorption properties than that of B2. Also, in the Langmuir model, the monolayer adsorption capacity (Q_m) of B1 was higher than that of B2. This may be explained by the porous structure of activated bentonite which is created by dissolution of the layer, so it caused an increase in the adsorption monolayer

capacity in the adsorption space of B1 pores. Finally, the order of suitability of adsorption isotherm models for adsorption of Ni^{2+} onto acid-activated bentonite is: Florry–Huggins > Langmuir > Freundlich > Temkin > Dubinin–Radushkevich. The order for natural bentonite is: Langmuir > Temkin > Freundlich > Florry–Huggins > Dubinin–Radushkevich.

5. CONCLUSION

New acid-activated bentonites were successfully prepared and characterized using SEM, XRD, FTIR, and BJH methods. The experimental adsorption capacity (12.5 mg/g) had the lowest difference with a calculated adsorption capacity for the pseudo-second-order kinetic model ($R^2 = 99$). Adsorption isotherms have been reported to have good fit with Langmuir and Florry–Huggins models based on experiments on adsorption of Ni(II) on natural and acid-activated bentonite. The best results from linear forms of the adsorption isotherm models for fitting the experimental data of natural bentonite are obtained for the Langmuir, Temkin and Freundlich models, while the results of fitting for acid-activated samples are Florry–Huggins, Langmuir and Freundlich, respectively. Although the results related to removal of Ni(II) on bentonite are significant and promising, a better understanding of the results is needed for future research regarding adsorbent properties such as swelling and surface active site quantifications.

ACKNOWLEDGEMENT

We acknowledge the critical reading of the manuscript and suggestions by Mr. H. Azimi, a Faculty Member of the Department of English Language and Literature of Shahid Beheshti University, Iran, and his invaluable comments and corrections that significantly improved the manuscript.

DATA AVAILABILITY STATEMENT

All relevant data are included in the paper or its Supplementary Information.

REFERENCES

Bhattacharyya, K. G. & Gupta, S. S. 2008 Uptake of Ni(II) ions from aqueous solution by kaolinite and montmorillonite: influence of acid activation of the clays. *Separation Science and Technology* **43** (11–12), 3221–3250.

Dada, A. O., Olalekan, A. P., Olatunya, A. M. & Dada, O. 2012 Langmuir, Freundlich, Temkin and Dubinin–Radushkevich isotherms studies of equilibrium sorption of Zn^{2+} unto phosphoric acid modified rice husk. *IOSR Journal of Applied Chemistry* **3** (1), 38–45.

Darvishi, Z. & Morsali, A. 2011 Synthesis and characterization of nano-bentonite by sonochemical method. *Ultrasonics Sonochemistry* **18** (1), 238–242.

García-Carvajal, C., Villarroel-Rocha, J., Curvale, D., Barroso, M. M. & Sapag, K. 2019 Arsenic (V) removal from aqueous solutions using natural clay ceramic monoliths. *Chemical Engineering Communications* **206** (11), 1440–14561.

Ghazizahedi, Z. & Hayati-Ashtiani, M. 2018 Removing Pb(II) by means of natural and acid-activated nanoporous clays. *IOP Conference Series: Materials Science and Engineering* **433**, 012069.

Ghomri, F., Lahsini, A., Laajeb, A. & Addaou, A. 2013 The removal of heavy metal ions (copper, zinc, nickel and cobalt) by natural bentonite. *Larhyss Journal* **12** (12), 37–54.

Hayati-Ashtiani, M. 2011 Characterization of nano-porous bentonite (montmorillonite) particles using FTIR and BET-BJH analyses. *Particle & Particle System Characterization* **28** (3–4), 71–76.

Hayati-Ashtiani, M. & Azimi, H. 2016 Characterization of different types of bentonites and their applications as adsorbents of Co(II) and Ni(II). *Desalination and Water Treatment* **57** (37), 17384–17399.

Hayati-Ashtiani, M., Jazayeri, S. H., Ghannadi, M. & Nozad, A. 2011 Experimental characterizations and swelling studies of natural and activated bentonites with their commercial applications. *Journal of Chemical Engineering Japan* **44** (2), 67–77.

Ijagbemi, C. O., Baek, M. H. & Kim, D. S. 2010 Adsorptive performance of un-calcined sodium exchanged and acid modified montmorillonite for Ni^{2+} removal: equilibrium, kinetics, thermodynamics and regeneration studies. *Journal of Hazardous Materials* **174** (1–3), 746–755.

Imran, M., Iqbal, M. M., Iqbal, J., Shah, N. S., Khan, Z. U. H., Murtaza, B., Amjad, M., Ali, S. & Rizwan, M. 2021 Synthesis, characterization and application of novel MnO and CuO impregnated biochar composites to sequester arsenic (As) from water: modeling, thermodynamics and reusability. *Journal of Hazardous Materials* **401**, 123338.

Iqbal, J., Shah, N. S., Sayed, M., Imran, M., Muhammad, N., Howari, F. M., Alkhoori, S. A., Khan, J. A., Khan, Z. U. H., Bhatnagar, A., Polychronopoulou, K., Ismail, I. & Haija, M. A. 2019 Synergistic effects of activated carbon and nano-zerovalent copper on the performance of hydroxyapatite-alginate beads for the removal of As^{3+} from aqueous solution. *Journal of Cleaner Production* **235**, 875–886.

Leroy, P., Weigand, M., Mériguet, G., Zimmermann, E., Tournassat, C., Fagerlund, F. & Kemna, A. 2017 Spectral induced polarization of Na-montmorillonite dispersions. *Journal of Colloid and Interface Science* **497**, 43–49.

Li, Z., Dong, H., Zhang, Y., Li, J. & Li, Y. 2017 Enhanced removal of Ni(II) by nanoscale zero valent iron supported on Na-saturated bentonite. *Journal of Colloid and Interface Science* **505**, 1093–1110.

Malamis, S. & Katsou, E. 2013 A review on zinc and nickel adsorption on natural and modified zeolite, bentonite and vermiculite: examination of process parameters, kinetics and isotherms. *Journal of Hazardous Materials* **252–253**, 428–461.

Ostovaritalab, M. A. & Hayati-Ashtiani, M. 2019 Investigation of Cs(I) and Sr(II) removal using nanoporous bentonite. *Particulate Science and Technology* **37** (7), 877–885.

Salem, A. & Karimi, L. 2009 Physico-chemical variation in bentonite by sulfuric acid activation. *Korean Journal of Chemical Engineering* **26**, 980–984.

Tang, S., Lin, L., Wang, X., Yu, A. & Sun, X. 2021 Interfacial interactions between collected nylon microplastics and three divalent metal ions (Cu(II), Ni(II), Zn(II)) in aqueous solutions. *Journal of Hazardous Materials* **403**, 123548.

Temuujin, J., Jadambaa, T., Burmaa, G., Erdenechimeg, S., Amarsanaa, J. & MacKenzie, K. J. D. 2004 Characterisation of acid activated montmorillonite clay from Tuulant (Mongolia). *Ceramics International* **30**, 251–255.

Yağmur, H. K. 2020 Synthesis and characterization of conducting polypyrrole/bentonite nanocomposites and in-situ oxidative polymerization of pyrrole adsorption of 4-nitrophenol by polypyrrole/bentonite nanocomposite. *Chemical Engineering Communications* **207** (8), 1171–1183.

First received 28 May 2021; accepted in revised form 21 September 2021. Available online 4 October 2021